Morphodynamic Tissues via Integrated Programmable Shape Memory Actuators

*Nikita Kalashnikov and Christopher Moraes**

Manipulating the shape of preformed living tissues can present a novel fabrication route toward complex biological architectures. However, external manipulation of tissues can be challenging to implement robustly at multiple length scales and with high degrees of freedom, particularly in soft fibrous tissue constructs. Here, a versatile platform is developed to drive soft tissue morphodynamics using embeddable shape memory actuators that generate multiscale, repetitive, and highly customized tissue deformation on demand. To achieve this, a thermally isolating coating technique is designed and developed for programmable shape memory wires, which protects surrounding biological materials from cytotoxic heating effects during wire actuation. The coated tissue actuators (CTAs) can then be embedded in engineered tissues and activated to produce both large- and small-scale tissue deformations in a highly customized and reproducible manner. Using this strategy, tissues can be forced to adopt specified shapes, with precise control over cell elongation and orientation within an encapsulating matrix. Furthermore, the system can produce predictable, highly localized, and customizable strains within fibrous matrices, capable of elongating cells and biasing their orientation within degrees of a desired direction. This strategy may hence have broad applicability in both applied tissue biofabrication and for fundamental studies of cell–matrix interactions.

1. Introduction

Origami is the art of folding paper into 3D shapes, and applying this strategy toward tissue engineering could create uniquely complex biological architectures.[1–6] This strategy could integrate two broad tissue engineering paradigms: cell-driven approaches in which the cells themselves direct and organize the tissue architecture; and externally driven strategies in which tissues are physically manipulated into desired shapes.[7] Cell-driven techniques allow highly scalable fabrication of complex structures that self-organize at the cellular length scale, such as lumens, branches, and buds.[8–11] In contrast, external manipulation of tissue shape allows precisely defined and robust control over larger length scale features, including cell position,[12–15] fluidic transport networks[16–19] and tissue form.[20–22] Combining these approaches by externally manipulating self-organizing cell-laden tissues would hence enable unique biofabrication and analytical possibilities.[23,24]

The central challenge in developing "morphodynamic" tissue engineering approaches is the difficulty in precisely handling living tissues on demand. While sufficiently large and rigid engineered tissues can be folded or rolled into tubes,[2] this requires manual skill for precision and consistency, is particularly challenging for soft fibrous materials, and any assisting rigs must be specifically designed to limit degrees of freedom (DOF) during actuation. Alternative techniques to form 3D structures include creating patterned prestress within materials[25–27] or designing hydrogels with differentially swellable regions,[28–30] such that the structures adopt predesigned 3D shapes. These techniques present limited options in terms of controlling the timing or reversibility of 3D shape actuation. More complex alternatives have also been proposed to change the shape of tissues including, leveraging the contractile activity of cells themselves by positioning cells at hinges between rigid plates,[1,5] culturing contractile cells on anisotropically flexible substrates,[31] or through cellular contraction of 3D collagen biomaterials.[3,32] Unfortunately, these strategies are not broadly applicable, as they exclude tissues that do not incorporate mechanically contractile cells, require certain cell and tissue spatial arrangements, and cannot be triggered on-demand to effect shape change at the appropriate time.

Smart materials could present a novel strategy to guide complex, on-demand, high DOF morphodynamics. These materials can change shape in response to a wide variety of orthogonal environmental stimuli, including heat, light, current, pressure and ionic imbalances, such as pH changes, calcium and enzymes.[33–39] Hence, as actuators, they can be designed to be triggered independently from cell activity in biological tissues. For example, Teshima et al.[40] and Stroganov et al.[41] recently developed composite polymers that can roll onto themselves and can either

N. Kalashnikov, Prof. C. Moraes
Department of Chemical Engineering
McGill University
Montreal, QC H3A 0C5, Canada
E-mail: chris.moraes@mcgill.ca
Prof. C. Moraes
Department of Biological and Biomedical Engineering
McGill University
Montreal, QC H3A 0C5, Canada
Prof. C. Moraes
Goodman Cancer Research Center
McGill University
Montreal, QC H3A 1A3, Canada

The ORCID identification number(s) for the author(s) of this article can be found under https://doi.org/10.1002/adfm.201903327.

ADVANCED
SCIENCE NEWS
www.advancedsciencenews.com

ADVANCED
FUNCTIONAL
MATERIALS
www.afm-journal.de

encapsulate suspended cells in 3D or convert a planar cell culture into a 3D cylindrical culture configuration. To date, these innovative strategies require specialized biomaterials, extensive fabrication steps, and are limited to one folding mechanism. Hence, while the conceptual approach of origami tissue engineering is simple, actuating the folding process to be generalizable, precise, on-demand, and biocompatible remains challenging.

In this work, we design and investigate smart material-based coated tissue actuators (CTAs) as a broadly applicable, robust, and versatile design strategy to induce both large and small morphodynamic changes in engineered tissues on demand. Shape memory wires can be programmed to generate large forces and adopt any selected shape via resistive heating of the material, deforming the surrounding tissue of interest into a desired shape. To prevent thermal damage to biological material during actuation, a thermal isolation coating technique was developed and validated. We then demonstrate and test the limits of the CTAs by deforming stiffness-tunable tissue phantoms and cell-laden collagen hydrogels, in terms of both large-scale deformations and finely tuned precise generation of local mechanical strains. These results demonstrate an ability to predictively control cell and tissue shape at multiple time- and length scales, suggesting broad utility of this morphodynamic tissue manipulation technology.

2. Results and Discussion

2.1. Materials Design Considerations

Nickel-titanium (NiTi) metal alloys are a well-established material system that can be initially formed into wires, springs, strips or plates, programmed to adopt a defined shape, and thermally actuated to return to that programmed shape on demand. NiTi alloys have previously been demonstrated to be compatible with a wide range of biomedical and implantable applications,[42–47] and can be actuated as needed via electrical resistance heating. They are also readily available with defined operating behaviors from several commercial sources. Furthermore, in contrast with alternative technologies such as shape memory polymers, NiTi wires can be easily programmed into a desired end-shape, can return to precisely defined positions on demand, and can generate large forces to achieve desired shape changes.[48] These characteristics make them an ideal choice with which to manipulate a variety of engineered tissues.

Three important criteria exist in selecting the type of NiTi wire for the proposed morphodynamic tissue handling and shape manipulation applications. First, the alloy characteristics of the NiTi material determines the required actuation temperature, which cannot exceed cell culture standards for the proposed applications. Second, intrinsic deformability of the material is important to ensure that the structures can be shaped easily under standard room temperature operating conditions. Third, the forces generated during actuation must be sufficient to deform tissues.

To meet these criteria using commercially available materials, we tested NiTi wires with transition temperatures of ≈45 °C and at "body temperature" (≈35 °C), available from Kellogg's Research Labs (Hudson, NH). 250 µm diameter wires

were selected to maximize the force that can be generated by the wire, maintain compatibility with the desired tissue sizes and shapes, and ensure that the wires are sufficiently flexible to allow positioning for programming. We confirmed that the selected wires could be physically restrained and heated to 450 °C for 1 h to program them into various shapes. Heating deformed wires in a water bath caused the wires to rapidly return to their programmed shapes, demonstrating the shape memory effect.

Although the "body temperature" wires would have been ideal for cell culture applications as they do not need to be heated beyond cell culture temperatures to initiate shape changes, our initial experiments demonstrated that the body-temperature wires were rigid and inflexible at room temperatures and could only be easily deformed at sub-zero temperatures. Since deforming the wires away from their programmed shape must be done without freezing the surrounding tissues, and the higher transition temperature wires were quite flexible at room temperature, 45 °C transition alloys would be required for tissue origami applications. Hence, we chose to develop an engineering strategy to protect the surrounding biological materials from heat damage during the thermal actuation process.

2.2. Finite Element-Based Modeling of Thermally Isolated Actuation Wires

To prevent heat damage to the surrounding tissue, we required a coating that is sufficiently flexible to allow deformation of the wire actuators, yet thermally and electrically isolating to prevent heat and charge transfer. Furthermore, the coating process must be readily applied to custom-designed wires for the technique to have broad applicability. To meet these criteria, we chose to develop a coating process for the silicone rubber polydimethylsiloxane (PDMS; Sylgard 184; Dow Corning), based on its biocompatibility,[49] low thermal conductivity (0.16–0.18 W m^{-1} K^{-1}),[50] historical use as an implantable encapsulant for electronics[51,52] and low, tunable mechanical rigidity (0.1 kPa to 1 MPa).[53]

A finite element model (**Figure 1**A) was developed to determine how the PDMS coatings could affect surface temperature during resistive heating of the NiTi actuation wire. As expected, both the NiTi wire core and the PDMS surface temperatures increased from room temperature when a step current load is applied. However, the surface temperature lags behind the core temperature because of the reduced thermal transport through the PDMS barrier layer. This lag period (defined as τ; Figure 1B, green highlight) is the available time window during which the core wire temperature will be at or above the 45 °C actuation temperature required to initiate shape changes, while the surface remains at cell-friendly temperatures (<37 °C). Hence, maximizing this safe actuation time window is of critical importance in applications involving deformation of live engineered tissues.

We reasoned that the safe actuation time window could be tuned by manipulating coating thickness, applied current, and pulsed stimulation protocols to create a sharp gradient from wire core to PDMS surface. Pulsed stimulation in which the system is allowed to cool toward room temperature during the
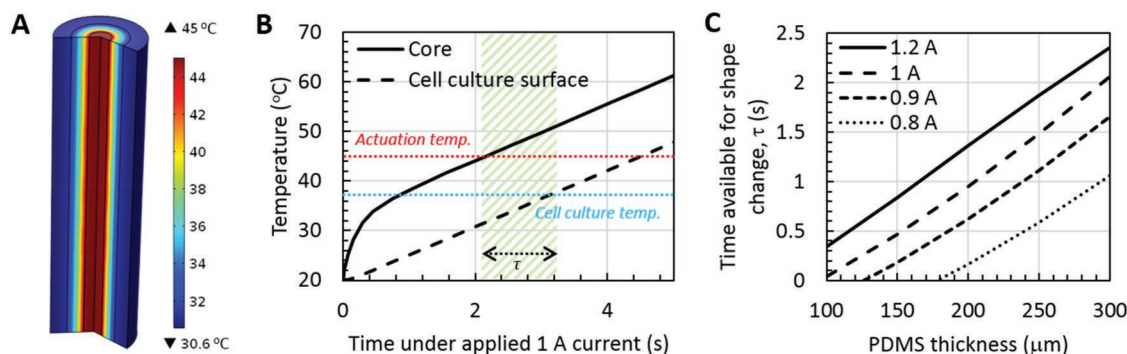
ADVANCED
SCIENCE NEWS
www.advancedsciencenews.com

ADVANCED
FUNCTIONAL
MATERIALS
www.afm-journal.de

Figure 1. Modeling of silicone coatings as a thermal barrier during resistive heating of smart material actuator wires. A) Temperature profile across and around the NiTi wire coated with a layer of PDMS. The wire was originally at room temperature and heated for ≈2 s with 1 ampere of current. B) Simulation data for the NiTi wire core and surface temperature of a 200 µm thick PDMS coating during resistive heating. τ indicates the safe actuation time window during which the temperature is sufficiently high to actuate the wire and low enough to prevent any adverse effect on cells. C) Parametric simulation of PDMS coating thickness and operating current on the safe actuation time window for selected operating parameters.

heating off-cycle was not suitable because PDMS has a comparatively high heat capacity and requires a longer cooling time than the NiTi core wire (Figure S1, Supporting Information). Fortunately, using constant current models, we found that the safe actuation time window would be on the order of seconds for 100 to 300 µm thick PDMS coatings. While thicker coatings would lead to increases in safe actuation time (Figure 1C), they would also limit the utility of this system as they make thicker constructs which then require additional force to deform during actuation. In contrast, thinner coatings would require more precise control over the timing of current flow, to shut off the current immediately after shape change is observed. Similarly, larger currents are advantageous as they cause a faster increase in core wire temperature, faster CTA deformation, and the longer dissipation times allow a larger safe actuation time window. However, currents larger than 1 ampere only minimally increased the safe actuation time window (<0.3 s) and required smaller total "on"-times, both of which would require stringent or feedback control over CTA operation. Hence, based on these simulations and competing constraints, we targeted a coating thickness of ≈200 µm and an operating current of 1 ampere for our experiments, as it provides a reasonable lag time of ≈1 s and a total allowable on-time of ≈3 s.

2.3. Development and Characterization of PDMS Coating Methods

Standard Sylgard 184 PDMS is most often cast and cured in slabs for potting or microfluidic applications. Obtaining conformal coatings hundreds of micrometers thick, directly on the cylindrical NiTi wires required the development of a novel coating process. Soft tubular PDMS structures have been previously fabricated by drawing an electrically heated metal filament through a PDMS pool and then releasing the cured PDMS coating from the wire through sonication.[54] We reasoned that rapid partial curing of PDMS on heated wires would provide a sufficiently polymerized template for subsequent complete curing in an oven. To achieve this, we prestretched and restrained NiTi wires to prevent reversion to the programmed state, immersed them in an unpolymerized

PDMS bath, and applied current to generate localized heat. Local polymerization of PDMS was initiated around the wire, producing a coating on the wire surface. The partially cured PDMS-coated wire was then removed from the bath, gently wiped with a Kimwipe to eliminate excess prepolymer, and completely cured in an oven for 1 h (**Figure 2**A).

Using this method, we achieved coatings that ranged from under 100 to 250 µm thick, through controlled resistive heating times (Figure 2B–D). The coatings were uniform across the length of the submerged wire, and reproducible between batches. For thicker coatings in particular, wires were not always perfectly centered within the PDMS, likely because of the effects of gravity on uncured polymer on the wire during the static curing step. To characterize this, we defined "offset" as the deviation of the wire from the central position of the PDMS material (exaggerated schematic in Figure 2E), which varied between 2 and 5% of the total construct diameter (Figure 2F). Together, these results demonstrate that the developed coating process is an effective strategy to create uniform thermally isolating barriers, with excellent control over coating parameters critical for the proposed applications.

2.4. Coated Tissue Actuator Operational Characteristics

To measure the force generation capabilities of the actuators, NiTi wires (250 µm diameter) were programmed into 6–8 cm long helical springs, straightened and coated with a ≈200 µm thick layer of PDMS to form CTAs. The CTAs were mounted on a vertical stand, deformed with hanging weights (10 to 70 grams) and then actuated to lift the suspended weights (**Figure 3**A–D). The tissue actuators were able to completely return to their programmed shape for loads less than 20 g or 200 mN, indicating that stresses as high as 4 MPa can be generated across the wire cross-section (Figure 3E). These results demonstrate that CTAs can provide sufficient forces to manipulate the shape of soft engineered tissues, which typically have rigidities on the order of tens of kPa.

The time required to initiate shape changes may also be an important characteristic for certain applications. Simulations with the selected 200 µm coating thickness were carried out
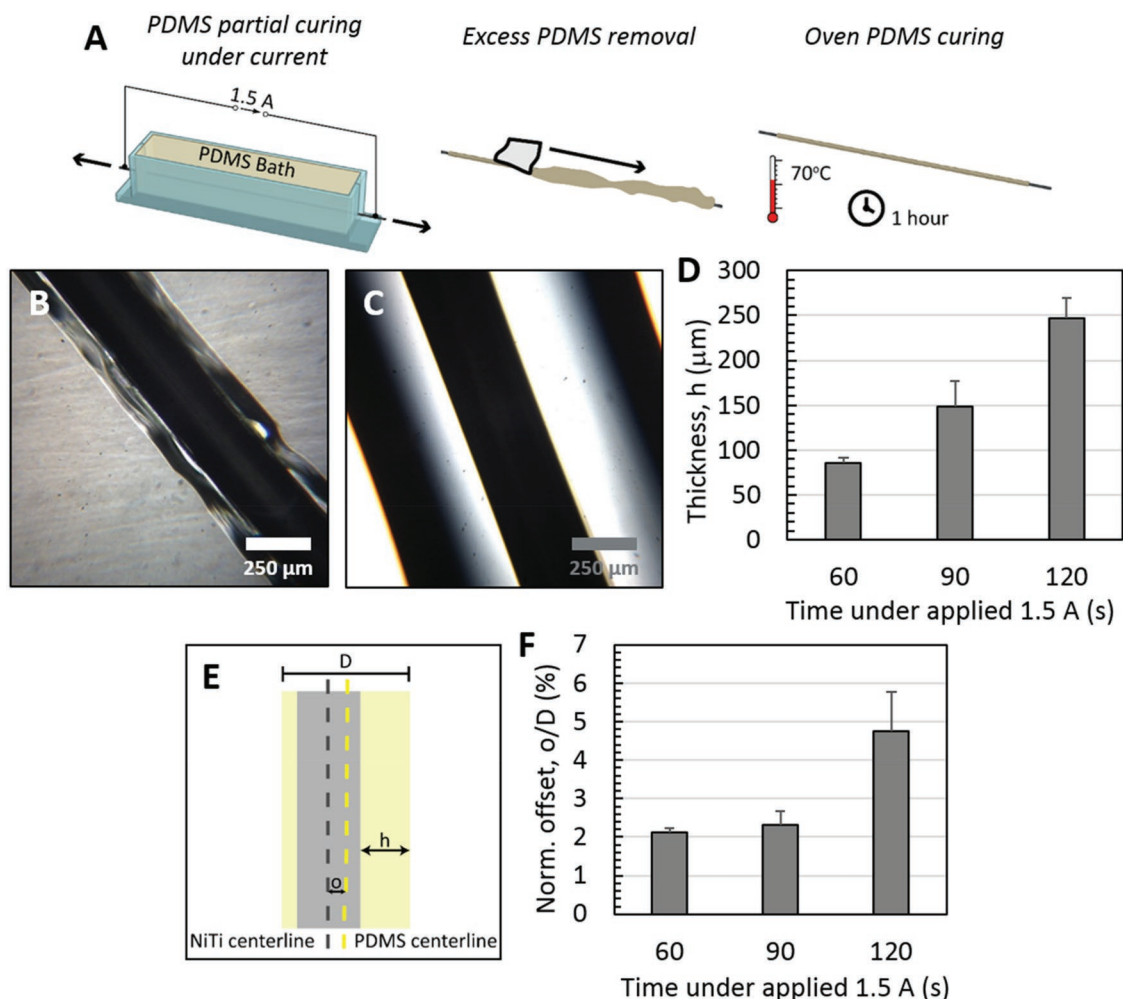
Figure 2. Development and characterization of the silicone coating process. A) Schematic of coating process. Nickel–titanium wires are immersed in a container containing uncured liquid PDMS and clamped at the edges to prevent shape change during heating. Applied current partially polymerizes PDMS. Excess PDMS is removed and the coating is cured. Cured PDMS coating on a NiTi wire after B) 60 s and C) 120 s of applied current. D) Measured coating thickness as a function of resistive heating time at 1.5 amperes. E) Schematic describing coating offset to characterize variations in coating uniformity around the NiTi wire, and F) offsets for measured coatings were characterized to less than 5% for all conditions tested. Data reported as mean ± standard error ($n = 3$).

to determine the current required to activate the tissue actuators (Figure 3F). As expected, lower currents (0.5 A) heated the wire more slowly than higher currents (1 A), and forced shape changes at ≈15 and ≈1 s, respectively. We then validated these models experimentally using a controlled-current source, and found strong agreement between the actuator deformation behavior and the model (Figure 3F). Hence, for the tissue actuators described here, we can initiate actuation within 1 s. Based on the time lag simulations (Figure 1C), this provides an acceptable current shut-off time delay of 1 s to avoid cytotoxic temperature effects.

2.5. Deformation of Stiffness-Tunable Tissue Phantoms

To determine the limits of the CTAs in deforming engineered tissues, we tested deformation of a tissue phantom in which the phantom stiffness could be modulated to mimic a wide range of

potential target tissues. Polyacrylamide is a well-established linear elastic hydrogel system that can be mechanically tuned over the physiological range of tissue modulus (10s of Pa to > 100 kPa), by adjusting the monomer to cross-linker ratios.[55] Furthermore, polyacrylamide can be readily integrated on PDMS surfaces using a benzophenone-mediated photografting techniques,[56] making it an ideal phantom material to probe the limits of tissue shape manipulation. Polyacrylamide hydrogels were loaded onto the benzophenone pretreated CTAs, using a custom 3D-printed mold to contain the liquid prepolymer. After UV-initiated polymerization, the composite polyacrylamide wire could be easily removed (**Figure 4**A). The produced hydrogels were relatively large (5 mm wide), easily released from the molding box, and grafted so strongly onto the PDMS surface that they could only be removed by destructive means.

To test the limits of the shape memory tissue actuation system, we developed a test case in which CTAs were programmed to adopt 60° bends, to create large and highly
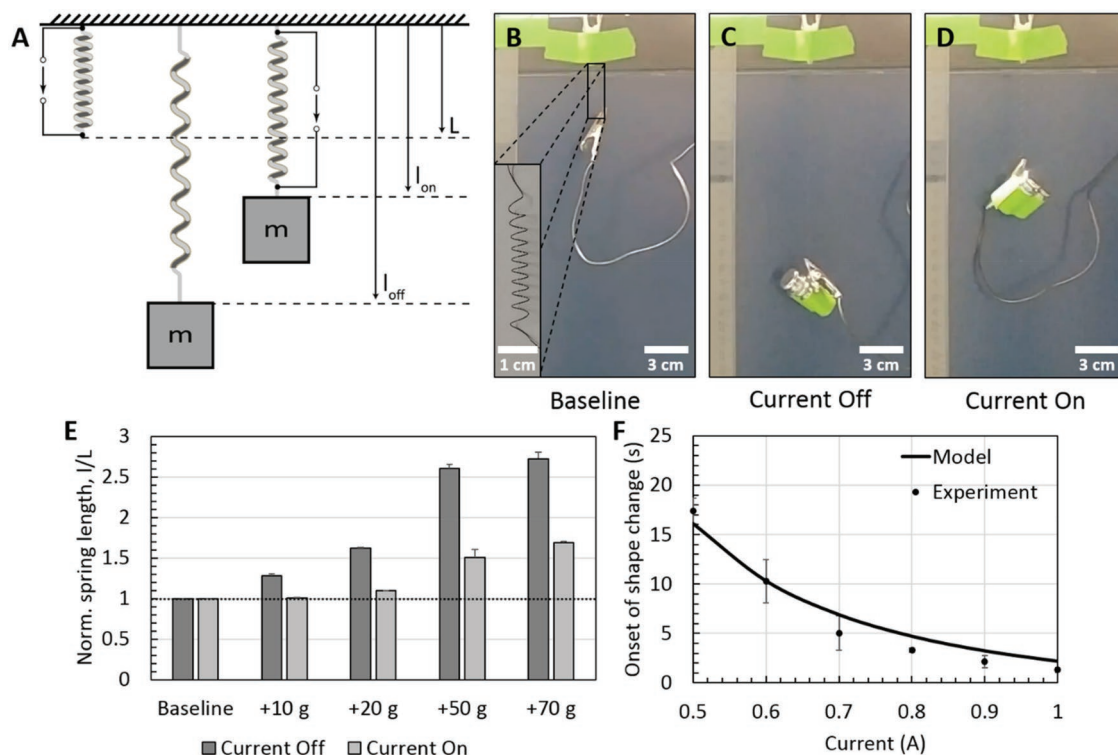
**ADVANCED
SCIENCE NEWS**
www.advancedsciencenews.com

**ADVANCED
FUNCTIONAL
MATERIALS**
www.afm-journal.de

Figure 3. Coated tissue actuator force-generating and shape recovery characteristics. A) Experimental schematic, illustrating CTA extension and recovery upon loading and actuation. B–D) 3 cm long springs with current-delivering connections at B) rest, C) applied load, and D) when actuated. E) Normalized spring extensions at various loads with and without current actuation. Dotted line represents unloaded programmed spring length. CTAs can completely restore programmed shape for loads of up to 20 g. F) The time to achieve shape change depends on applied current, matching computational predictions for resistive heating of CTAs. Data reported as mean ± standard deviation ($n = 3$).

localized stresses in the surrounding tissue. The programmed wires were straightened, coated in PDMS and grafted to the polyacrylamide phantoms (Figure 4A). CTAs were then activated and the extent to which they folded could be measured through image analysis (Figure 4B–D). To demonstrate that CTAs are capable of robust and repeated return to their programmed configurations when embedded in tissues, polyacrylamide phantom-coated CTAs were manually straightened and actuated over multiple cycles. The wires demonstrated robust return to their expected programmed shape for at least 15 cycles (Figure 4E), demonstrating the utility of this approach for repeated tissue deformations.

When the actuating current was turned off, phantom-embedded CTAs exhibited a slight recoil toward an unfolded straight-line position (Figure 4F). This was not observed for bare NiTi wires, which reliably returned to their programmed positions and maintained these positions when resistive heating was stopped, but the 200 µm thick PDMS coating itself limits the actuator return to the programmed 60° angle. CTAs were consistently able to achieve 80° bends. No recoil toward the original straight configuration was observed when the wires were cooled, indicating that the restoring force of the PDMS coating is negligible. Phantom tissues of 0.3 and 0.9 kPa stiffness did not affect the performance characteristics of the CTAs, but higher stiffness phantoms (>4.8 kPa) did limit angular bending, and also introduced a small recoil component at the highest levels of tissue stiffness tested (Figure 4C,D).

The angle-bending test case was designed to generate high levels of localized stress at a point within the tissue phantoms, as a limiting test case for CTA deformation. To confirm that the observed bending limitations are due to high local stresses in the tissues, we also programmed NiTi wires to form circles of various curvatures (radii = 13, 6, and 1 mm). These shapes should distribute stresses more uniformly throughout the tissue phantom. Actuated wires faithfully returned to their programmed shape for larger radius circles, but circles with radii of 1 mm were not able to completely return to their programmed position (Figure 4G). These folding limitations were highly reproducible and repeatable, which indicates that they can be accounted for in the initial programming step of the NiTi wire; and these limitations apply primarily when engineered tissues are stiffer than 5 kPa. Together, these results demonstrate that the geometry, mechanics, and size of the biomaterial scaffold could play a role in limiting the wire's ability to return to its programmed shape, and that this effect is reproducible and hence can be accounted for when designing and programming the CTA.

2.6. Viable Manipulation of Living Soft-Tissue Constructs

To demonstrate biocompatibility, CTAs were integrated into live engineered tissues. The collagen contraction process is a well-established mechanism by which fibroblasts can compact a low-density collagen gel, producing tissues with cells that form
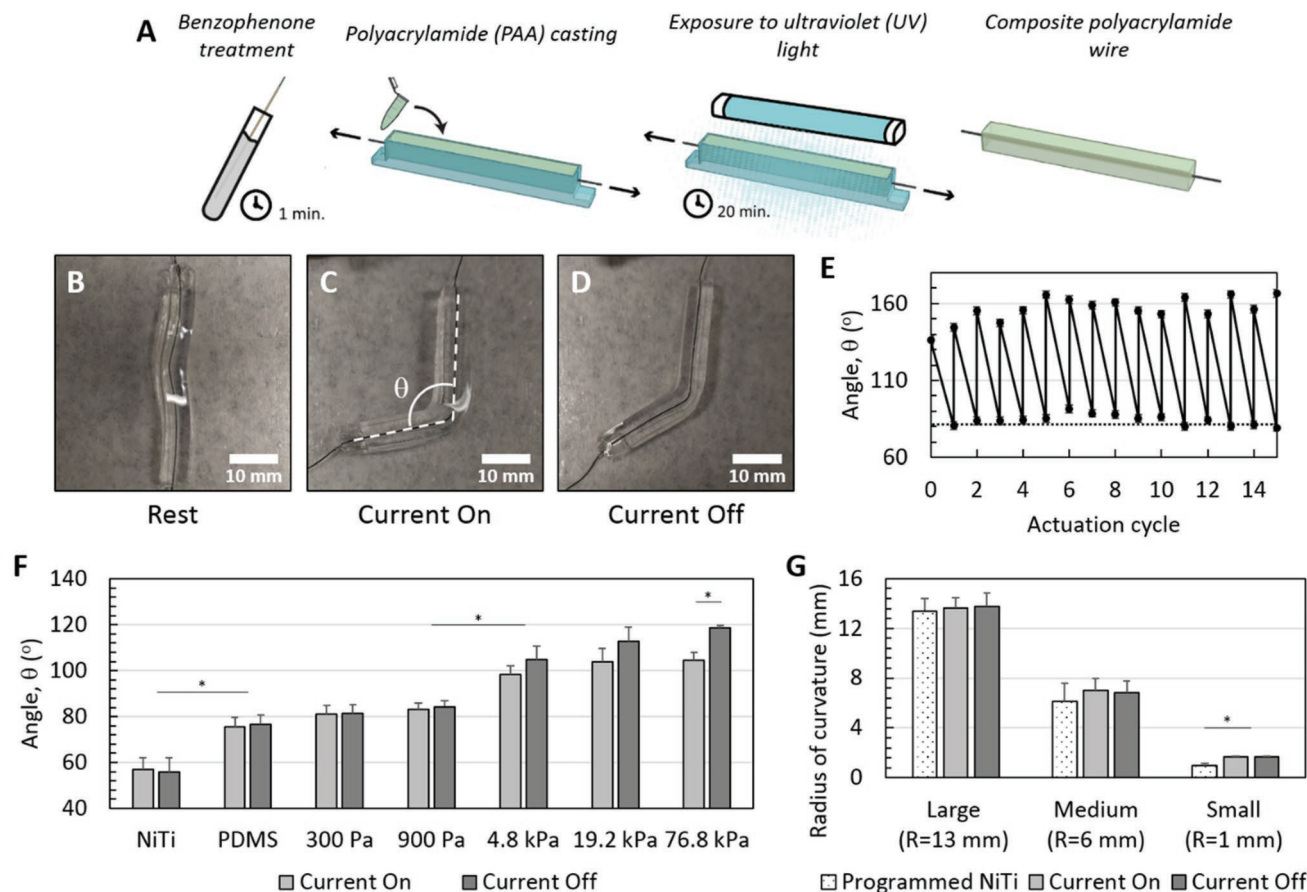
Figure 4. Deformation of stiffness-tunable tissue phantoms. A) Fabrication process for a polyacrylamide tissue phantom around an embedded coated tissue actuator. CTAs are functionalized with benzophenone and then cast within a polyacrylamide hydrogel and cross-linked under UV light. B–D) Programmed phantom CTAs are shown here B) at rest, C) under applied current, and D) after current is turned off. E) Wire bend angles measured during repeated manual straightening and actuated bending of the 900 Pa phantom-embedded CTA wire. The construct reliably returns to its expected angle (dashed line) over 15 actuation cycles. Data presented as mean ± estimated measurement error. F) Measured wire bend angle for phantom-embedded CTAs. The PDMS coating, and stiffer tissue phantoms limits CTA return to the programmed angle. The stiffest tissue phantoms tested (>75 kPa) also exhibit a statistically significant recoil effect in which the CTA further straightens after applied current is removed. G) Measured radius of curvature for different programmed circular shapes demonstrate that local stresses within the deforming tissues contribute to the CTA limitations in achieving desired shapes. Data presented as mean ± standard error ($n = 3$; $*$ $p < 0.05$).

well-spread, aligned structures in a physically tense matrix.[57–60] Here, a model HS-5 bone marrow fibroblast cell line was used to contract a collagen matrix around a CTA (**Figure 5**A). The collagen gels densified around the wires over time due to fibroblast activity (Figure 5B,C), confirming viability and functional activity of the cells in tissues containing CTAs. Cells were maintained for one week in culture, during which time they further compacted the tissue (Figure 5D), adopting elongated morphologies along the wires, and developing a filamentous actin network within the tissue (Figure 5E), consistent with previous studies of cell contraction around a standard wire.[61] Resistive heating of the wires deformed the collagen into pre-programmed helical structures (Figure 5F,G), demonstrating the capacity of this system to precisely manipulate and deform soft and delicate biological structures; and produce complex large-scale shapes and orientations in soft engineered tissues. The aligned and deformed cells can now be encapsulated in a second biomaterial, affording the ability to create complex control over cell alignment within engineered tissues (Figure 5H).

Live/dead assays for cell viability were performed before and after resistive heating (Figure 5I,J) confirming that cells survive the shape transition. To further confirm that cells survive the heating process, we applied current continuously for an additional 5 s after shape transition. Extended resistive heating should raise the surface temperatures above 37 °C. No significant difference in viability was observed even after this unnecessary heating (Figure 5K). These results demonstrate that the designed coating is sufficient to protect cells and tissues from any heat generated during actuation.

2.7. Defined and Reproducible Local Strains in Biomaterials with CTAs

Handling soft tissues such as cell-laden collagen gels presents significant challenges, particularly for applications in which precise manipulation of the tissue is needed to understand fundamental cell–matrix interactions. For example, externally
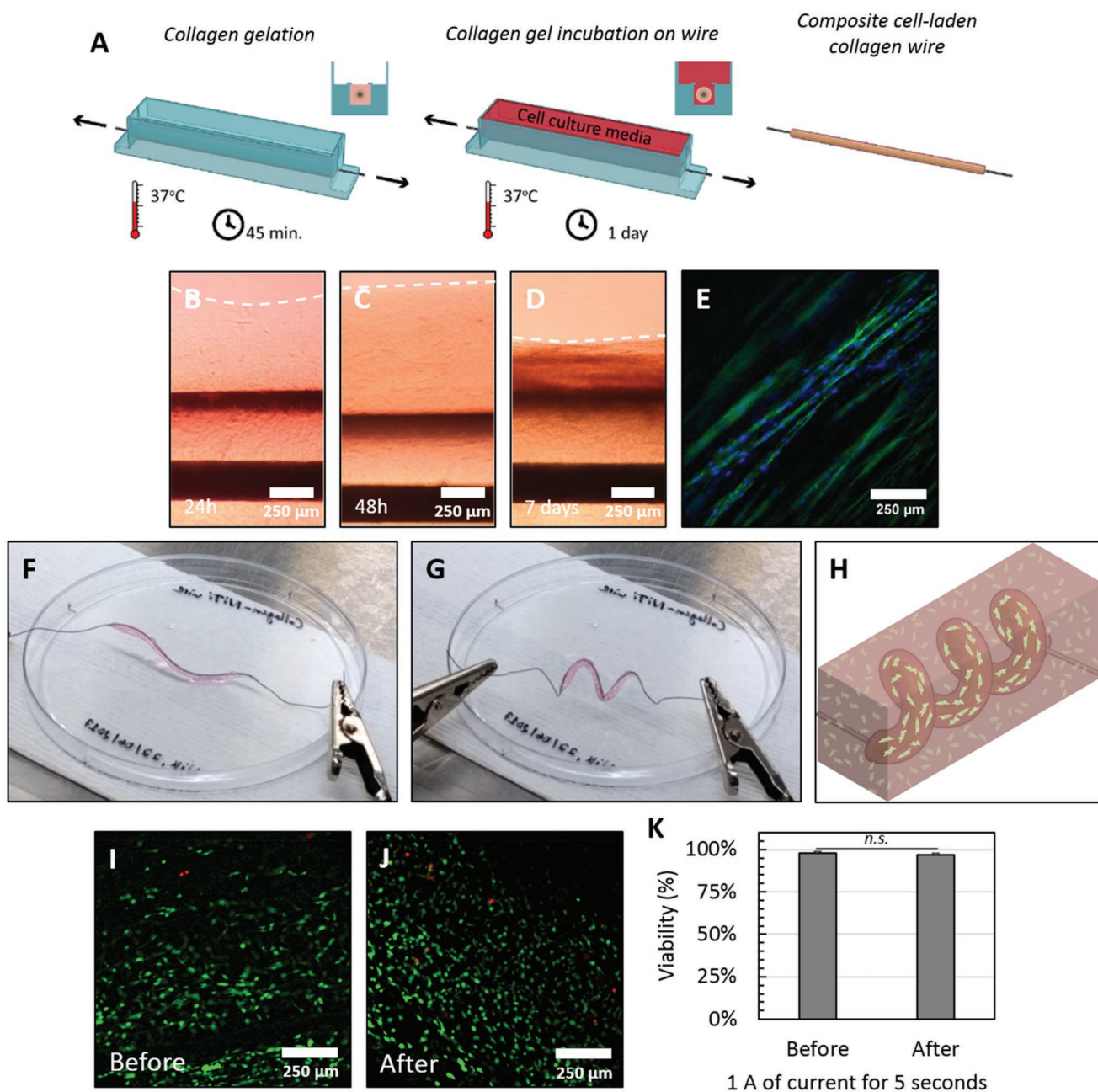
ADVANCED
SCIENCE NEWS
www.advancedsciencenews.com

ADVANCED
FUNCTIONAL
MATERIALS
www.afm-journal.de

Figure 5. CTA-deformation of condensed cell-laden collagen tissues. A) Experimental schematic for fabrication of composite CTA-collagen devices. Bright field microscope images of a composite collagen wire as it densifies around the CTA at B) 24 h, C) 48 h, and D) 7 d of culture. White dashed lines indicate the collagen tissue edge. E) Confocal fluorescent microscope image highlighting tissue actin structure in condensed collagen gels (green = phalloidin actin; blue = DAPI nuclear label). F) Construct at rest and G) actuated to fold into a 5 cm long helical structure. H) Illustration of a composite collagen wire embedded in a second biomaterial, highlighting the potential capacity of this system to control cell morphology within engineered tissues. Representative live-dead assay microscope images I) before and J) after tissue shape change (green = calcein AM live stain; red = ethidium homodimer dead stain). K) No measurable changes were observed in cell viability after extended heating. Data presented as mean ± standard deviation, ($n = 3$, n.s. $p > 0.05$).

applied strains are well-established to direct and specify cell phenotypes, including cell alignment and nuclear morphology, which are known to direct cellular programs such as migration[62,63] and differentiation.[64–66] However, creating small and well-defined strains, particularly in soft biomaterials, often requires the development of specialized culture systems.[67–70]

Here, we apply CTAs to create small and precisely defined strains within very soft, cell-laden collagen gels in a highly reproducible manner.

To generate small strains on demand, two parallel CTAs were embedded in cell-laden, collagen; and actuated to apply a differential strain profile across the collagen tissue prior to
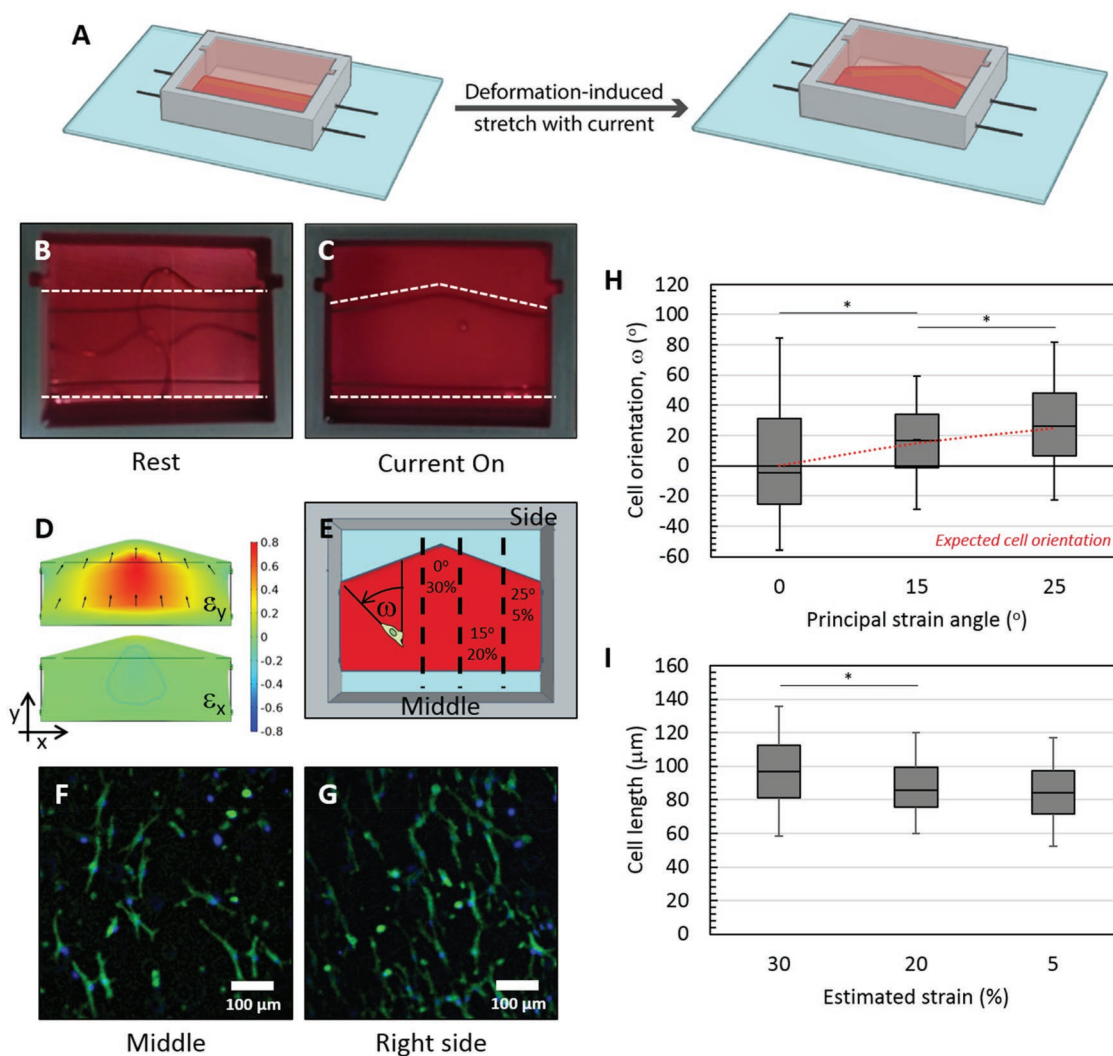
**ADVANCED
SCIENCE NEWS**
www.advancedsciencenews.com

**ADVANCED
FUNCTIONAL
MATERIALS**
www.afm-journal.de

Figure 6. Precisely defined strains created within 3D engineered tissues using CTAs. A) Conceptual experimental schematic. Images of wires and integrated collagen gels at B) initial and C) final configurations after current application (white dashed lines indicate wire position). D) Finite element analysis of the strain field created within the construct. Black arrows represent the direction of principal strain. E) Analysis schematic detailing angular coordinate frame for measurement, and regions analyzed in these experiments. Representative confocal fluorescent images of cells located at the F) middle and G) side of the tissue (scale bar 100 µm, green = phalloidin actin; blue = DAPI nuclear label). (H) Cell orientation across the strained tissue (boxplots represent median, interquartile range and 1.5x the interquartile range; red dotted line represents the angle of principal strain). I) Measured cell length across the strained tissue. Data presented as mean ± standard deviation, ($n = 100$–200 cells, $*p < 0.05$).

contraction (**Figure 6**A–C). As a first demonstration, we forced one wire to adopt a triangular shape (Figure 6B,C) deforming the tissue. This pattern creates tension along the vertical axis and compression along the horizontal axis, in a manner that changes across the length of the tissue, which can be predicted using simple finite element modeling (Figure 6D). In the middle region of the device, strains are large (≈30%), and the principal strain is aligned along the vertical angle, while on the sides of the device, strains are small (≈5%), but the principal strain is offset by 25° from the vertical.

Prior to actuation, cells exhibited a preferential orientation perpendicular to the parallel CTAs across all regions of the device, as expected based on previous studies of cell alignment in an anchored collagen matrix.[70] Cell orientation and elongation were measured immediately after actuation to observe the effects of this applied strain, and were found to be significantly different in various regions of the fibrous matrix (Figure 6F–H), and matched the strain fields in terms of both orientation and elongation. The median orientation of cells within the collagen matrix tracked closely with the direction of principal strain, and was significantly different across the device (Figure 6H). This is consistent with cells being repositioned within the fibrous matrix based on CTA-induced deformation of that matrix.

Interestingly, cell elongation was significantly increased in the central regions of 30% strain, but not at 20% strain or lower (Figure 6I). This reflects the idea that cells are being mechanically elongated due to their adhesion with strained collagen fibers, and the nonlinear relationship between cell elongation and tissue strain indicates a complex mechanical relationship between cell elongation and tissue deformation. This is

**ADVANCED
SCIENCE NEWS**

www.advancedsciencenews.com

**ADVANCED
FUNCTIONAL
MATERIALS**

www.afm-journal.de

consistent with previous studies of cell–matrix deformation[68] in which low-stress deformation of a soft extracellular matrix shields strain transfer to stiffer embedded objects such as cells. Only at higher strain levels is the applied stress sufficient to deform the embedded cells.

These small but statistically significant differences emerged only after quantitative analysis, demonstrating the capacity of this technique to make small changes to cells within tissues. These results confirm that the directional orientation of cells can be manipulated with even low levels of applied strain, consistent with previous studies that replicate these findings using substantially more complex tissue manipulation setups.[67,71] Hence, this simple application demonstrates the capacity for this system to make precise, repeatable changes in soft, living matter, and to precisely tune orientation and morphology of embedded cells within the tissue, demonstrating the potential for CTAs in studies of fundamental cell and tissue mechanobiology with high spatial and morphological resolution.

2.8. Future Applications and Technical Limitations

This robust and inexpensive technique makes it possible to precisely deform and manipulate soft tissues in a reproducible manner on demand, at various stages of tissue maturation. This technique could have immediate applications in technologies such as the Tumor Roll for Analysis of Cellular Environment and Response,[72] a tightly rolled sheet of engineered tissue that can be used to create dense hypoxic tissues, and unrolled for easy imaging and analysis; or in emerging origami-based tissue engineering applications in which morphodynamic control over tissues is needed to achieve desired tissue architectures. This would be particularly advantageous when engineering complex tissues with multiple cell types; as multicellular patterning can be readily achieved on flat 2D substrates,[73–75] which can then be folded into desired configurations to create 3D tissues that would not be possible with other technologies.

CTAs do have some limitations to consider. First, they are designed to remain in the tissue, which may limit their utility particularly in the design of implantable tissues. However, they do enable on-demand, and high force actuation of tissues via an electrical switch; whereas biodegradable or resorbable alternatives such as certain shape memory polymers generate lower forces, and require significant pH or temperature changes to stimulate actuation, which are challenging to apply in vivo. Hence, we envision the primary applications of this system to be for in vivo engineered models.

Second, this technique is limited in potential for miniaturization. While NiTi wires could certainly be custom-manufactured to be thinner, and with predefined programmed features, the deformation forces produced will decrease with wire diameter. Hence, a careful balance must be struck between the minimal coating thickness needed to thermally isolate the wire, and the ability of the NiTi wire to deform this coating. These issues may be addressed by modifying the thermal coefficient of the PDMS coating by doping it with nonconductive particles and using a timed stimulation strategy (Figure S1, Supporting Information) to produce thinner silicone coatings.

Third, the present configuration of tissue actuators only allows transition toward one programmed shape. Developing multistable configurations would enable a wide variety of dynamic experiments such as cyclic cell stretching and complex tissue reconfiguration on demand. Theoretically, this could be achieved with the CTAs by positioning multiple actuator wires within the tissue that have been programmed to adopt different states. Resistance heating of each wire would then force the overall system into a known configuration, allowing multistable operation for dynamic actuation applications.

3. Conclusion

CTAs provide a simple and attractive method to morphodynamically manipulate soft, living, delicate, tissues into desired shapes and structures. The electrically driven shape-changing mechanism generates high forces, and allows on-demand actuation of biological structures. The simple silicone coating method developed through localized resistive heating could be broadly applicable to a variety of fabrication purposes, and in this application provides sufficient thermal and electrical isolation to protect biological tissues from temperature and currents needed to generate tissue shape changes. Using this system, tissues can be allowed to mature in one configuration, allowing precise and predictive development of spread and aligned cellular morphologies; and then actuated to force those cells into a desired structure. These prespread and aligned cells can then be integrated into other biomaterials to produce customized tissues with control over cell spreading vectors in 3D. Furthermore, we demonstrate the use of this platform technology to engineer shape-changing tissues, in which small applied strains can be used to readily direct cell orientation on demand. Broadly, the use of such actuators provides a novel design strategy with which to enable advanced manufacturing strategies that provide morphodynamic control over tissue structures.

4. Experimental Section

Unless otherwise stated, all cell culture materials and supplies were purchased from Fischer Scientific (Ottawa, ON) and chemicals from Sigma-Aldrich (Oakville, ON). All data analysis was performed in EXCEL including the one-sided and two-sided *t*-tests for significance (*p*-values thresholds for each test are listed in the figure's associated caption).

Shape Memory Alloy Programming: Nitinol (NiTi; Kellogg's Research Labs; Hudson, NH, USA) wires with a diameter of 250 µm were used to create the coated tissue actuators. Each wire was programmed to a specific shape with a simple heat treatment. The shape of the wire was set by weaving it through a stainless steel mesh (TWP Inc; Berkley, CA, USA) or wrapped around a generic screw, both of which also acted as a rigid support. These constructs were heated up to 450 °C in a microwave furnace (MAS 700, CEM) for 1 h, and then taken out of the furnace and left outside until they cooled back down to room temperature. The austenite start and finish temperatures corresponding to the NiTi transformation temperature range were also recorded by observing the shape memory effect triggered by slowly heating the wire in a water bath.

Modeling Resistive Heating of Coated Wires: A 2D axisymmetric model was built in COMSOL v.5.3.1.201 (Comsol Inc.; Burlington, MA, USA) to study the temperature evolution in a model soft tissue construct during actuation with current (Figure 1A). Current passing through the NiTi material (6450 kg m^{-3}, 320 J kg^{-1} K^{-1}, 0.16 W m^{-1} K^{-1},

Table 1. Polyacrylamide formulations to produce phantom tissues of increasing stiffness.

Nominal stiffness [kPa]	0.3	0.9	4.8	19.2	76.8
Acrylamide [wt%]	3	3	7.5	7.5	12
Bisacrylamide [wt%]	0.049	0.085	0.054	0.236	0.241

and 1316 kS m^{-1}) led to resistive heating and the associated wire temperature increase acted as a driving force for heat transfer to the surroundings through the PDMS coating (970 kg m^{-3}, 1460 J kg^{-1} K^{-1} and 8.6 W m^{-1} K^{-1}) and the collagen (modeled as water). In terms of boundary conditions, a current density equivalent to 1 A was applied at one end of the wire, which was grounded at the other end, and electrical insulation was enforced at the wire-PDMS boundary. Both types of physics were then coupled together with the wire acting as an electrical heat source. The ends of the PDMS coating were thermally insulated, forcing the heat generated by the wire straight through the collagen model material as a thermal outflow boundary condition. A mapped quad mesh was used with a mesh element size set to be ≈2% of the total construct thickness (50 elements), which ensured that the coefficient of variation was less than 1%. Parameter sweeps were performed on the coating thickness and the applied current to determine their impact on the coating surface temperature and on the actuation time.

PDMS Coating Process: A regulated constant-current power supply (Lambda LP-410A-FM) was used to pass a current of 1.5 A through a wire suspended in a degassed 10:1 monomer/curing agent Sylgard 184 PDMS mixture (Dow Corning) bath (Figure 2A). The local high temperature near the wire caused partial curing of the PDMS. The excess liquid PDMS was then carefully removed with a Kimwipe and the coating was left to fully cure by placing the wire into a 70 °C oven for 1 h. During the coating process, the wire was held under mechanical tension to prevent any shape change from occurring. The PDMS container was designed in AutoCAD (Autodesk) and 3D printed using an Ember printer (Autodesk).

Mechanical Testing with Stiffness-Tunable Polyacrylamide Hydrogels: To fabricate the composite polyacrylamide wires, the coated NiTi wires were first impregnated with benzophenone[56] by submerging the PDMS-coated wire in a 10% benzophenone solution (35:65 (w/w) water/acetone solvent) for 1 min. Excess benzophenone was washed off of the wire with methanol. Each coated wire was then placed inside of a 3D printed mold (Autodesk Ember 3D printer). It was held under tension with two clamps on each side of the container. The mold was then filled with a polyacrylamide (PAA) solution prepared beforehand according to recipes presented in detail elsewhere.[55] Briefly, precursor polyacrylamide hydrogel solutions were prepared by mixing acrylamide (Bio-rad, 1610140) with bisacrylamide (Bio-rad, 1610141) at a desired ratio (**Table 1**) in phosphate buffered saline (PBS). Then, to polymerize 900 µL of precursor PAA solution, 100 µL of 1% (w/v) ammonium persulfate (APS; Bio-rad, 1610700) in PBS was added along with 1.5 µL of tetramethylethylenediamine (TEMED) catalyst to the PAA base solution. This construct was then exposed to UV for ≈20 min to allow the PAA to chemically bond to the PDMS coating. The polymerized composite polyacrylamide wire was then carefully peeled out of its mold (Figure 4A).

Cell Culture and Staining: Human bone marrow fibroblasts (HS-5, ATCC) were used as a model cell line in these experiments. Cells were grown in Dulbecco's modified Eagle's medium (DMEM; Gibco) supplemented with 10% fetal bovine serum (FBS) and 1% antibiotic-antimycotic at 37 °C and 5% CO$_2$. Cells were harvested with trypsin and collected in cell culture media containing trypsin inhibitors to be then passage in a new T-flask or used for the fabrication of the soft tissue constructs. The live-dead assay was performed with calcein AM and ethidium homodimer-1 stains (Life Technologies; Carlsbad, CA, USA). The soft constructs were incubated for 1 h in 8 × 10^{-6} M calcein AM and 4 × 10^{-6} M ethidium homodimer-1. Samples where stained for F-actin and nuclei for 3 h using a 1:200 dilution of FITC phalloidin and

Table 2. Collagen hydrogel components used as a model tissue.

	Volume [µL]
10X DMEM	20
1 M sodium hydroxide (NaOH)	4.5
Sterile water	15.5
7.5% sodium bicarbonate (NaHCO$_3$) buffer	10
1X DMEM	50
3 mg mL^{-1} bovine collagen type I (VWR)	150
Cell suspension	50
Final 1.5 mg mL^{-1} collagen gel volume	300

a 1:1000 dilution of Hoechst 33258 in 1% bovine serum albumin (BSA) stock solutions.

Microscopy and Image Analysis: Bright field images of the wires at 4× magnification were obtained with a Motic AE21 inverted microscope, equipped with a Canon camera (Figure 2B,C/Figure 5B–D). An Olympus IX-73 spinning disk confocal microscope was used for the fluorescent images (Figure 5E,H,I/6F,G). All other images were obtained with a handheld camera. Image analysis was performed with ImageJ (FIJI; ver. 1.51s; National Institute of Health, USA). A Gaussian blur filter and dark field background subtraction were applied, followed by brightness/contrast adjustments to improve cell visibility. Cell viability was quantified by manually counting the fraction of live/dead cells in *n* = 3 samples. Cell morphology was analyzed by freehand outlining the cells in each image and then running an analysis for Feret length and angle.

Soft Tissue Construct Fabrication: The soft constructs were fabricated following a similar casting procedure as employed for the composite polyacrylamide wires. The coated NiTi wire was held in place inside of a PDMS mold with two clamps at both sides of the mold (Figure 5A). A previously made collagen-cell mixture (**Table 2**) was then poured into the mold and allowed to gel for 45 min inside of an incubator. Cell culture media was then added to the mold's upper chamber. After a day of culture, the constructs were easily taken out of the mold and further incubated in a Petri dish filled with media. The PDMS mold was produced by replica molding from a 3D printed piece. A modified version of this fabrication process was employed to produce the construct used for stretching. A biocompatible 3D printed frame (36 mm by 28.5 mm polylactic acid; Monoprice select mini V2 printer) glued to a glass slide was used instead of the PDMS mold. The 3D printed frame featured two small slits through which a smaller glass slide could be introduced as a divider (Figure 6B,C). This made it possible to cast the gel around the two wires and then to perform the shape change within the same container by removing the divider after a day of culture. During culture, clamps were used to fix the wires within the gel (Figure 6B), but are then removed before actuating the stretch (Figure 6C). Tissues were fixed immediately after actuation for subsequent analysis of cell orientation and morphology.

Stretch Deformation Modeling: A 3D soft construct stretch model was also built in COMSOL v.5.3.1.201 (Comsol Inc.; Burlington, MA, USA) (Figure 6D). The top wire (84 GPa) was gradually ramped up to assume the same shape observed during the stretch experiment (Figure 6C) with a prescribed displacement boundary condition while the bottom wire was restricted from deforming using a fixed domain constraint. During this simulated shape change, the soft construct model material was deformed accordingly. The contact between the collagenous tissue and the wires was modeled with identity boundary pairs, essentially imposing a bond between both materials. The tissue was modeled as a 1 kPa linear elastic material with a Poisson's ratio of 0.13 and density of 1 g cm^{-3}. A free tetrahedral mesh was used with a mesh element size set to be ≈5% of the total tissue width (20 elements), which ensured that the coefficient of variation was less than 1%. The mesh element quality was maintained above 0.8 at all times.

Supporting Information

Supporting Information is available from the Wiley Online Library or from the author.

Acknowledgements

Conflict of Interest

The authors declare no conflict of interest.

Keywords

[1] K. Kuribayashi-Shigetomi, H. Onoe, S. Takeuchi, *PLoS One* **2012**, *7*, e51085.

[2] S.-H. Kim, H. R. Lee, S. J. Yu, M.-E. Han, D. Y. Lee, S. Y. Kim, H.-J. Ahn, M.-J. Han, T.-I. Lee, T.-S. Kim, S. K. Kwon, S. G. Im, N. S. Hwang, *Proc. Natl. Acad. Sci. USA* **2015**, *112*, 15426.

[3] A. J. Hughes, H. Miyazaki, M. C. Coyle, J. Zhang, M. T. Laurie, D. Chu, Z. Vavrušová, R. A. Schneider, O. D. Klein, Z. J. Gartner, *Dev. Cell* **2018**, *44*, 165.

[4] M. S. Sakar, B. M. Baker, *Dev. Cell* **2018**, *44*, 131.

[5] Q. He, T. Okajima, H. Onoe, A. Subagyo, K. Sueoka, K. Kuribayashi-Shigetomi, *Sci. Rep.* **2018**, *8*, 4556.

[6] V. A. Bolaños Quiñones, H. Zhu, A. A. Solovev, Y. Mei, D. H. Gracias, *Adv. Biosyst.* **2018**, *2*, 1800230.

[7] V. D. Varner, C. M. Nelson, *Annu. Rev. Chem. Biomol. Eng.* **2014**, *5*, 507.

[8] H. Mori, N. Gjorevski, J. L. Inman, M. J. Bissell, C. M. Nelson, *Proc. Natl. Acad. Sci. USA* **2009**, *106*, 14890.

[9] C. Wei, M. Larsen, M. P. Hoffman, K. M. Yamada, *Tissue Eng.* **2007**, *13*, 721.

[10] K. Tanner, H. Mori, R. Mroue, A. Bruni-Cardoso, M. J. Bissell, *Proc. Natl. Acad. Sci. USA* **2012**, *109*, 1973.

[11] Y. Sasai, *Nature* **2013**, *493*, 318.

[12] M. Nakamura, A. Kobayashi, F. Takagi, A. Watanabe, Y. Hiruma, K. Ohuchi, Y. Iwasaki, M. Horie, I. Morita, S. Takatani, *Tissue Eng.* **2005**, *11*, 1658.

[13] Y. Nahmias, D. J. Odde, *Nat. Protoc.* **2006**, *1*, 2288.

[14] G. M. Akselrod, W. Timp, U. Mirsaidov, Q. Zhao, C. Li, R. Timp, K. Timp, P. Matsudaira, G. Timp, *Biophys. J.* **2006**, *91*, 3465.

[15] J. A. Park, S. Yoon, J. Kwon, H. Now, Y. K. Kim, W.-J. Kim, J.-Y. Yoo, S. Jung, *Sci. Rep.* **2017**, *7*, 14610.

[16] D. Therriault, S. R. White, J. A. Lewis, *Nat. Mater.* **2003**, *2*, 265.

[17] A. P. McGuigan, M. V. Sefton, *Proc. Natl. Acad. Sci. USA* **2006**, *103*, 11461.

[18] L. M. Bellan, S. P. Singh, P. W. Henderson, T. J. Porri, H. G. Craighead, J. A. Spector, *Soft Matter* **2009**, *5*, 1354.

[19] J. S. Miller, K. R. Stevens, M. T. Yang, B. M. Baker, D.-H. T. Nguyen, D. M. Cohen, E. Toro, A. A. Chen, P. A. Galie, X. Yu, R. Chaturvedi, S. N. Bhatia, C. S. Chen, *Nat. Mater.* **2012**, *11*, 768.

[20] J. Yeh, Y. Ling, J. M. Karp, J. Gantz, A. Chandawarkar, G. Eng, J. Blumling III, R. Langer, A. Khademhosseini, *Biomaterials* **2006**, *27*, 5391.

[21] G. R. Souza, J. R. Molina, R. M. Raphael, M. G. Ozawa, D. J. Stark, C. S. Levin, L. F. Bronk, J. S. Ananta, J. Mandelin, M.-M. Georgescu, J. A. Bankson, J. G. Gelovani, T. C. Killian, W. Arap, R. Pasqualini, *Nat. Nanotechnol.* **2010**, *5*, 291.

[22] J. Lee, A. A. Abdeen, K. L. Wycislo, T. M. Fan, K. A. Kilian, *Nat. Mater.* **2016**, *15*, 856.

[23] D. Rodenhizer, E. Gaude, D. Cojocari, R. Mahadevan, C. Frezza, B. G. Wouters, A. P. McGuigan, *Nat. Mater.* **2016**, *15*, 227.

[24] R. Derda, A. Laromaine, A. Mammoto, S. K. Y. Tang, T. Mammoto, D. E. Ingber, G. M. Whitesides, *Proc. Natl. Acad. Sci. USA* **2009**, *106*, 18457.

[25] M. Jamal, N. Bassik, J.-H. Cho, C. L. Randall, D. H. Gracias, *Biomaterials* **2010**, *31*, 1683.

[26] B. Yuan, Y. Jin, Y. Sun, D. Wang, J. Sun, Z. Wang, W. Zhang, X. Jiang, *Adv. Mater.* **2012**, *24*, 890.

[27] R. Arayanarakool, A. K. Meyer, L. Helbig, S. Sanchez, O. G. Schmidt, *Lab Chip* **2015**, *15*, 2981.

[28] J. Kim, J. A. Hanna, M. Byun, C. D. Santangelo, R. C. Hayward, *Science* **2012**, *335*, 1201.

[29] M. Jamal, S. S. Kadam, R. Xiao, F. Jivan, T.-M. Onn, R. Fernandes, T. D. Nguyen, D. H. Gracias, *Adv. Healthcare Mater.* **2013**, *2*, 1142.

[30] E. Käpylä, S. M. Delgado, A. M. Kasko, *ACS Appl. Mater. Interfaces* **2016**, *8*, 17885.

[31] J. Sang, X. Li, Z. Shao, Z. Li, J. Fu, *ACS Biomater. Sci. Eng.* **2017**, *3*, 2860.

[32] X. Zhang, Z. Meng, J. Ma, Y. Shi, H. Xu, S. Lykkemark, J. Qin, *Small* **2015**, *11*, 3666.

[33] Y. Zhang, F. Zhang, Z. Yan, Q. Ma, X. Li, Y. Huang, J. A. Rogers, *Nat. Rev. Mater.* **2017**, *2*, 17019.

[34] W. M. Huang, C. L. Song, Y. Q. Fu, C. C. Wang, Y. Zhao, H. Purnawali, H. B. Lu, C. Tang, Z. Ding, J. L. Zhang, *Adv. Drug Delivery Rev.* **2013**, *65*, 515.

[35] T. van Manen, S. Janbaz, A. A. Zadpoor, *Mater. Today* **2018**, *21*, 144.

[36] A. Lendlein, H. Jiang, O. Jünger, R. Langer, *Nature* **2005**, *434*, 879.

[37] X. Shen, C. Viney, E. R. Johnson, C. Wang, J. Q. Lu, *Nat. Chem.* **2013**, *5*, 1035.

[38] M. Ma, L. Guo, D. G. Anderson, R. Langer, *Science* **2013**, *339*, 186.

[39] L. Brannon-Peppas, N. A. Peppas, *Chem. Eng. Sci.* **1991**, *46*, 715.

[40] T. F. Teshima, H. Nakashima, Y. Ueno, S. Sasaki, C. S. Henderson, S. Tsukada, *Sci. Rep.* **2017**, *7*, 17376.

[41] V. Stroganov, J. Pant, G. Stoychev, A. Janke, D. Jehnichen, A. Fery, H. Handa, L. Ionov, *Adv. Funct. Mater.* **2018**, *28*, 1706248.

[42] J. Ryhänen, E. Niemi, W. Serlo, E. Niemelä, P. Sandvik, H. Pernu, T. Salo, *J. Biomed. Mater. Res.* **1997**, *35*, 451.

[43] S. Kujala, A. Pajala, M. Kallioinen, A. Pramila, J. Tuukkanen, J. Ryhänen, *Biomaterials* **2004**, *25*, 353.

[44] C. M. Schirmer, C. B. Heilman, *Neurosurg. Focus* **2011**, *30*, E8.

[45] K. R. Dai, X. K. Hou, Y. H. Sun, R. G. Tang, S. J. Qiu, C. Ni, *Injury* **1993**, *24*, 651.

[46] R. Uflacker, J. Robison, *Eur. Radiol.* **2001**, *11*, 739.

[47] Y. Sakaguchi, T. Sato, Y. Muranishi, Y. Yutaka, T. Komatsu, K. Omori, T. Nakamura, H. Date, *J. Thorac. Cardiovasc. Surg.* **2018**, *156*, 1264.

[48] D. Vokoun, V. Kafka, C. T. Hu, *Smart Mater. Struct.* **2003**, *12*, 680.

[49] M.-C. Bélanger, Y. Marois, *J. Biomed. Mater. Res.* **2001**, *58*, 467.

[50] H.-S. Chuang, S. Wereley, *J. Micromech. Microeng.* **2009**, *19*, 045010.

[51] A. C. Richards Grayson, R. Scheidt Shawgo, Y. Li, M. J. Cima, *Adv. Drug Delivery Rev.* **2004**, *56*, 173.

[52] S. H. Kim, J.-H. Moon, J. H. Kim, S. M. Jeong, S.-H. Lee, *Biomed. Eng. Lett.* **2011**, *1*, 199.

[53] C. Moraes, J. M. Labuz, Y. Shao, J. Fu, S. Takayama, *Lab Chip* **2015**, *15*, 3760.

[54] W. Xi, F. Kong, J. C. Yeo, L. Yu, S. Sonam, M. Dao, X. Gong, C. T. Lim, *Proc. Natl. Acad. Sci. USA* **2017**, *114*, 10590.

[55] J. R. Tse, A. J. Engler, *Curr. Protoc. Cell Biol.* **2010**, *47*, 10.16.1.

[56] C. S. Simmons, A. J. S. Ribeiro, B. L. Pruitt, *Lab Chip* **2013**, *13*, 646.

[57] E. Bell, B. Ivarsson, C. Merrill, *Proc. Natl. Acad. Sci. USA* **1979**, *76*, 1274.

[58] E. Bell, H. P. Ehrlich, D. J. Buttle, T. Nakatsuji, *Science* **1981**, *211*, 1052.

[59] Z. Feng, M. Yamato, T. Akutsu, T. Nakamura, T. Okano, M. Umezu, *Artif. Organs* **2003**, *27*, 84.

[60] C. Moraes, A. B. Simon, A. J. Putnam, S. Takayama, *Biomaterials* **2013**, *34*, 9623.

[61] S. S. Nunes, J. W. Miklas, J. Liu, R. Aschar-Sobbi, Y. Xiao, B. Zhang, J. Jiang, S. Massé, M. Gagliardi, A. Hsieh, N. Thavandiran, M. A. Laflamme, K. Nanthakumar, G. J. Gross, P. H. Backx, G. Keller, M. Radisic, *Nat. Methods* **2013**, *10*, 781.

[62] P. Friedl, K. Wolf, J. Lammerding, *Curr. Opin. Cell Biol.* **2011**, *23*, 55.

[63] N. Von Offenberg Sweeney, P. M. Cummins, E. J. Cotter, P. A. Fitzpatrick, Y. A. Birney, E. M. Redmond, P. A. Cahill, *Biochem. Biophys. Res. Commun.* **2005**, *329*, 573.

[64] M. Wabitsch, R. E. Brenner, I. Melzner, M. Braun, P. Möller, E. Heinze, K.-M. Debatin, H. Hauner, *Int. J. Obes.* **2001**, *25*, 8.

[65] J. Sanchez-Esteban, L. A. Cicchiello, Y. Wang, S.-W. Tsai, L. K. Williams, J. S. Torday, L. P. Rubin, *J. Appl. Physiol.* **2001**, *91*, 589.

[66] S. Saha, L. Ji, J. J. de Pablo, S. P. Palecek, *Biophys. J.* **2008**, *94*, 4123.

[67] D. Vader, A. Kabla, D. Weitz, L. Mahadevan, *PLoS One* **2009**, *4*, e5902.

[68] C. Moraes, G. Wang, Y. Sun, C. A. Simmons, *Biomaterials* **2010**, *31*, 577.

[69] C. Moraes, R. Zhao, M. Likhitpanichkul, C. A. Simmons, Y. Sun, *J. Micromech. Microeng.* **2011**, *21*, 054014.

[70] R. Zhao, T. Boudou, W.-G. Wang, C. S. Chen, D. H. Reich, *Adv. Mater.* **2013**, *25*, 1699.

[71] M. Eastwood, V. C. Mudera, D. A. Mcgrouther, R. A. Brown, *Cell Motil.* **1998**, *40*, 13.

[72] D. Rodenhizer, D. Cojocari, B. G. Wouters, A. P. McGuigan, *Biofabrication* **2016**, *8*, 045008.

[73] A. Bernard, E. Delamarche, H. Schmid, B. Michel, H. R. Bosshard, H. Biebuyck, *Langmuir* **1998**, *14*, 2225.

[74] A. Folch, M. Toner, *Biotechnol. Prog.* **1998**, *14*, 388.

[75] E. A. Roth, T. Xu, M. Das, C. Gregory, J. J. Hickman, T. Boland, *Biomaterials* **2004**, *25*, 3707.